Mesh Construction with Prescribed Properties near Boundary

Boris Azarenok

Dorodnicyn Computing Center of Russian Academy of Sciences, Moscow, Russia
azarenok@ccas.ru

Summary. A quasi-conformal mapping of the parametric domain onto the underlying physical domain is used to generate a 2D structured mesh with required properties: grid line orthogonality and prescribed mesh point clustering near the domain boundary. The functions implementing the mapping are sought by solving the Dirichlet problem for the elliptic partial differential equations. An additional control for the cell shape is executed by introducing a local mapping. Example of the mesh near the airfoil is presented.

Keywords: structured mesh; elliptic grid generation; control metric

1 Introduction

When constructing a structured (block-structured) mesh on a two-dimensional domain with aim to simulate viscous gas flow near a body, there are additional requirements imposed on the mesh. It is grid line orthogonality and prescribed strong mesh point clustering near the streamline body. If the outside domain boundary is in “infinity” and may have an arbitrary shape, then one may use algorithms based on solving hyperbolic partial differential equations (PDEs) (cf. [1, 2]). If the entire boundary is stringently defined, such methods are badly applicable due to the boundary value problem (BVP) is ill-possed. Besides, the hyperbolic PDEs transfer singularities of the solution (i.e., breaks on the boundary) along characteristics. Quasilinear hyperbolic PDEs may produce a non-smooth and even discontinuous solution even with smooth boundary conditions [3].

For the rigidly defined boundary it is convenient to utilize elliptic PDEs of the second order (cf. [4, 5, 6]) producing meshes at a quasi-conformal mapping. Here it is sought a mapping of the domain $\mathcal{P}$ in the parametric plane with a given square mesh onto the domain Ω in the physical plane where the grid is required. We call $\mathcal{P}$ a parametric domain and Ω is called a physical domain. If to employ a homeomorphic mapping $\mathbf{F}:\mathcal{P}\rightarrow\Omega$ then the image of the square mesh on $\mathcal{P}$ is an unfolded grid on Ω. For the Laplace equations, the Radó theorem [7] asserts that the harmonic mapping of a simply connected bounded domain onto a simply connected bounded convex domain is univalent subject to a given homeomorphism between the boundaries. To satisfy the conditions of the Radó theorem for nonconvex physical domains, the inverted Laplace equations are applied (cf. [4, 6]). The use of the inverted Laplace equations provides a smooth and quasiuniform grid. However, the grid so generated is not always satisfactory in the sense that points may not be clustered to where they are needed and grid orthogonality near the domain boundary is not supported. Besides, some problem arises at discrete level that leads to mesh folding (cf. [8, 9, 10, 11]).

In [5], with purpose to implement grid line control, a substitution of variables was implemented for the inverted Laplace equations. In [12], the source terms were used in those Eqs. and, in [16], an algorithm of specifying coefficients in source terms was suggested to impose grid line orthogonality and prescribed mesh point clustering near the domain boundary. An additional algebraic transformation was applied in [13], additional local mapping was executed in [14, 10]. It is not possible to obtain orthogonal mesh in the entire domain with a curvilinear boundary, except simple canonical domains (disk, ring or their sector, etc.) because the BVP is ill-possed [15]. In complicated domains, the mesh, generated by using a conformal mapping, is not applicable for mathematical simulation. On the other hand, one may obtain a mesh with orthogonal grid lines of one family towards the boundary and prescribed mesh point clustering near the domain boundary. To this end, in the source terms of the Poisson equations of [12] it is specified coefficients at the exponent by solving an inverse problem [16]. This process is rather cumbersome and practical calculation demonstrates that grid line may approach the boundary at an angle substantially differing from 90^o [16, 2, 17].

We present the grid generation method based on solving the Dirichlet problem for the elliptic PDEs [10, 11]. Grid line control is imposed by introducing an additional local mapping which induces the control metric. We present the way of specifying the control metric with aim of obtaining grid line orthogonality and required mesh point clustering near the domain boundary. Example of the mesh near the NACA6409 airfoil is considered.

2 Grid generation using mapping

Let a structured mesh be required on a simple connected domain Ω represented as a curvilinear quadrangle in the plane of physical variables x, y. The mesh is defined by the nodal Cartesian coordinates

$$\mathbf{r}_{i,j} = (x, y)_{i,j}\ , \quad i = 1, 2, \ldots, N_1,\ j = 1, 2, \ldots, N_2,$$

subject to given nodal coordinates on the boundary $\partial\Omega$

$$\mathbf{r}_{i,1},\, \mathbf{r}_{i,N_2},\ i{=}1,\ldots,N_1;\quad \mathbf{r}_{1,j},\, \mathbf{r}_{N_1,j}\ j{=}1,\ldots,N_2.$$

To this end, the parametric domain $\mathcal{P}$, rectangle with the sides $N_1{-}1$ and $N_2{-}1$ subdivided into unit squares, in the plane ξ,η is mapped onto the physical domain Ω. If a homeomorphic mapping $\mathbf{F}:\mathcal{P}\to\Omega$ can be found, the image of the square mesh on the domain $\mathcal{P}$ will be an unfolded mesh on the domain Ω. This is true at least in continuous approach. Meantime at the discrete level, truncation error may case grid folding (cf. [11, 9, 8]). As grid lines on Ω it is utilized the equipotential lines of the functions $\xi(x,y)$ and $\eta(x,y)$.

The functions $\mathbf{F}{=}\mathbf{x}(\boldsymbol{\xi}){=}(x(\xi,\eta),y(\xi,\eta))$, of class $\mathbb{C}^2$, executing the mapping $\mathbf{x}(\boldsymbol{\xi}):\mathcal{P}\to\Omega$ (see Fig. 1), are sought by solving the Dirichlet problem for the elliptic PDEs [10, 11]

$$\begin{aligned}\mathcal{L}(x) = g_{22}x_{\xi\xi} - 2g_{12}x_{\xi\eta} + g_{11}x_{\eta\eta} - x_\xi\big[\tilde G_{22}(P-Q) + \tilde G_{12}(S-R)\big] \quad (1)\\ -x_\eta\big[\tilde G_{11}(R-S) + \tilde G_{12}(Q-P)\big] = 0, \qquad \mathcal{L}(y) = 0,\end{aligned}$$

$$\tilde G_{kl} = \frac{G_{kl}}{\sqrt{\det G}}\,,\quad P = g_{11}\frac{\partial \tilde G_{12}}{\partial\eta} - g_{12}\frac{\partial \tilde G_{11}}{\partial\eta},\quad Q = \frac12\Big(g_{11}\frac{\partial \tilde G_{22}}{\partial\xi} - g_{22}\frac{\partial \tilde G_{11}}{\partial\xi}\Big),$$
$$S = g_{12}\frac{\partial \tilde G_{22}}{\partial\xi} - g_{22}\frac{\partial \tilde G_{12}}{\partial\xi},\quad R = \frac12\Big(g_{11}\frac{\partial \tilde G_{22}}{\partial\eta} - g_{22}\frac{\partial \tilde G_{11}}{\partial\eta}\Big).$$

The components of the metric tensor g_{kl}, induced by the mapping $\mathbf{x}(\boldsymbol{\xi})$, are

$$g_{11} = x_\xi^2 + y_\xi^2,\quad g_{12} = x_\xi x_\eta + y_\xi y_\eta,\quad g_{22} = x_\eta^2 + y_\eta^2\,.$$

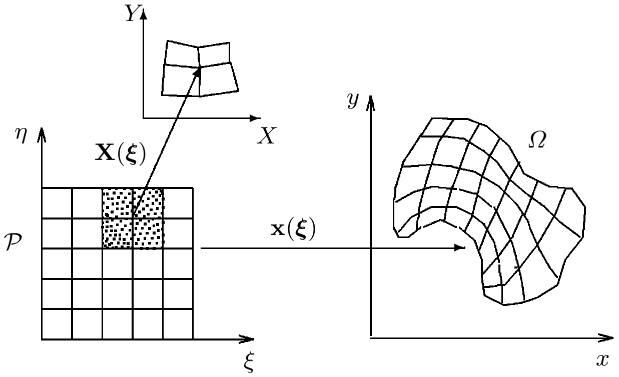

Fig. 1. Mapping $\mathbf{x}(\boldsymbol{\xi}):\mathcal{P}\to\Omega$ is sought by solving problem (1),(2). Control metric G is specified by local mapping $\mathbf{X}(\boldsymbol{\xi})$, e.g., 4 cells (dotted) in plane ξ,η onto 4 cells in plane X,Y.

In Eqs. (1), we use one more metric G. The control metric G is induced by a local mapping $\mathbf{X}(\boldsymbol{\xi})$ of a subdomain $\mathcal{P}_1{\subset}\mathcal{P}$ to a domain in the plane of new variables X,Y. At discrete level it may be, for instance, four adjacent cells in the parametric plane ξ, η, forming a 9-point stencil to approximate the system (1), onto four adjacent cells in the plane X, Y (see Fig. 1). The components of the control metric tensor G_{kl} are

$$G_{11} = X_\xi^2 + Y_\xi^2, \quad G_{12} = X_\xi X_\eta + Y_\xi Y_\eta, \quad G_{22} = X_\eta^2 + Y_\eta^2 \ .$$

The boundary conditions specify the boundary correspondence

$$x = x_b(\xi, \eta) \ , \quad y = y_b(\xi, \eta), \quad (\xi, \eta) \in \partial\mathcal{P}. \tag{2}$$

The mapping $\mathbf{x}(\boldsymbol{\xi})$ is quasi-conformal, i.e., it transforms an infinitesimal circle of $\mathcal{P}$ to an infinitesimal ellips of Ω.

In some particular cases, the mapping $\mathbf{x}(\boldsymbol{\xi}) : \mathcal{P} \to \Omega$ is a composition of two sequential mappings. First, we construct the mapping $\mathbf{X}(\boldsymbol{\xi})$ of the domain $\mathcal{P}$ onto the domain $\mathcal{C}$ in the plane X, Y (see Fig. 2). Therefore, a mesh (or a part of the mesh) is constructed on the domain $\mathcal{C}$. Next the image of this mesh is obtained on the domain Ω at the mapping $\mathbf{x}(\mathbf{X}) : \mathcal{C} \to \Omega$. If G_{kl} is the identity tensor, then Eqs. (1) turn to the inverted Laplace equations of [4] and $\mathbf{x}(\boldsymbol{\xi}) : \mathcal{P} \to \Omega$ is the inverse harmonic mapping. By the Radó theorem [7], the direct harmonic mapping $\boldsymbol{\xi}(\mathbf{x}) : \Omega \to \mathcal{P}$, specified by the Laplace equations, is univalent.

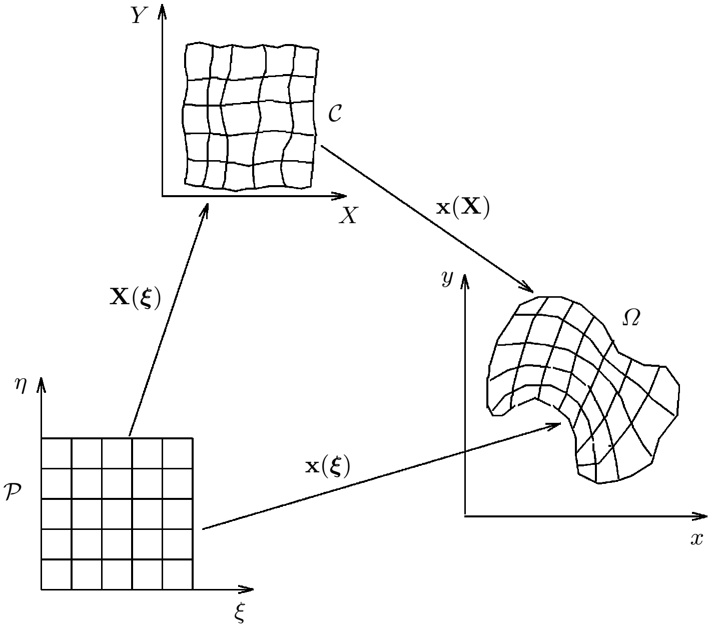

Fig. 2. In particular cases, first mapping $\mathbf{X}(\boldsymbol{\xi}) : \mathcal{P} \to \mathcal{C}$ is used and then mapping $\mathbf{x}(\mathbf{X}) : \mathcal{C} \to \Omega$ is considered.

PDEs (1) are the Euler equations to the universal functional suggested in [14]. The property of universality implies that by specifying the control metric

G any given smooth homeomorphic mapping $\mathbf{F}:\mathcal{P}\to\Omega$ may be reproduced by solving the problem (1),(2) and, at discrete level, any given unfolded mesh may by constructed. In addition, Eqs. (1) are invariant to nonsingular transformations of the coordinates x, y and X, Y. These two properties of Eqs. (1) allow to obtain a grid with required properties subject to such a grid exists.

3 Discretization and numerical solution

Eqs. (1) are approximated to second order at the interior mesh node (i, j) on the domain $\mathcal{P}$ via the difference relations on the 9-point square stencil of spacing 1. The derivatives of the function $x(\xi, \eta)$ are approximated as follows

$$\begin{aligned}
&x_\xi \approx [x_\xi]_{i,j} = 0.5(x_{i+1,j} - x_{i-1,j}),\ x_\eta \approx [x_\eta]_{i,j} = 0.5(x_{i,j+1} - x_{i,j-1}),\\
&x_{\xi\xi}\approx[x_{\xi\xi}]_{i,j}=x_{i+1,j} - 2x_{i,j} + x_{i-1,j},\ x_{\eta\eta}\approx[x_{\eta\eta}]_{i,j}=x_{i,j+1} - 2x_{i,j} + x_{i,j-1},\\
&x_{\xi\eta} \approx [x_{\xi\eta}]_{i,j} = 0.25(x_{i+1,j+1} - x_{i+1,j-1} - x_{i-1,j+1} + x_{i-1,j-1}),
\end{aligned} \tag{3}$$

and the components of the metric tensor g_{kl} are approximated as follows

$$[g_{11}]_{i,j} = [x_\xi]^2_{i,j} + [y_\xi]^2_{i,j}\ ,\quad [g_{22}]_{i,j} = [x_\eta]^2_{i,j} + [y_\eta]^2_{i,j}\ ,$$

$$[g_{12}]_{i,j} = [x_\xi]_{i,j}[x_\eta]_{i,j} + [y_\xi]_{i,j}[y_\eta]_{i,j}\ .$$

The components of the control metric tensor G_{kl} are approximated similarly.

Substituting these relations into Eqs. (1) gives approximation of the operators $\mathcal{L}(x)$ and $\mathcal{L}(y)$ denoted $[\mathcal{L}(x)]_{i,j}$ and $[\mathcal{L}(y)]_{i,j}$, respectively. The resulting discretized equations with boundary conditions (2) are solved by employing the iterative procedure. Let nodal coordinates be known at the lth iteration. Then at the l+1th iteration they are updated by formulae [5]

$$x^{l+1}_{i,j} = x^l_{i,j} + \tau\frac{[\mathcal{L}(x)]_{i,j}}{2([g_{11}]_{i,j} + [g_{22}]_{i,j})},\quad y^{l+1}_{i,j} = y^l_{i,j} + \tau\frac{[\mathcal{L}(y)]_{i,j}}{2([g_{11}]_{i,j} + [g_{22}]_{i,j})}. \tag{4}$$

Here [.] denotes approximation of the underlying expression at the node (i, j) at the lth iteration, iterative parameter $0<\tau<2$. To accelerate convergence of the iterations (4) the Seidel procedure is employed. Iterations are executed until the condition for the nodal coordinates $\mathbf{r}_{i,j}=(x, y)_{i,j}$

$$\max_{i,j} |\mathbf{r}^{l+1}_{i,j} - \mathbf{r}^l_{i,j}| < \varepsilon,\quad i=2,\dots,N_1-1,\ j=2,\dots,N_2-1,$$

is satisfied. Here $\varepsilon>0$ is sufficiently small. As an initial guess $\mathbf{r}^o_{i,j}$ one may utilize a grid provided by the inverted Laplace equations.

4 Control metric assignment

The control metric G is specified so that the grid possesses required properties. Suppose we need to construct a mesh with the j-line (equipotential line $\xi(x,y)$=$const$) approaching orthogonally the upper part of the boundary $\partial\Omega$ (where the nodes (i,N_2), i=$1,2,\ldots,N_1$, are located) and, in addition, with prescribed mesh point clustering near this part of $\partial\Omega$. In other words, several upper i-lines (equipotential line $\eta(x,y)$=$const$), say j_o, are given by the nodal coordinates $\mathbf{r}_{i,j}$=$(x,y)_{i,j}$

$$\mathbf{r}_{i,j} = \mathbf{r}_{i,j+1} + \mathbf{n}_{i,j+1} h_{i,j+1/2},\ i{=}2,\ldots,N_1{-}1,\ j{=}N_2{-}1,\ldots,N_2{-}j_o, \quad (5)$$

where the spacing $h_{i,j+1/2}$ is the distance between the nodes (i,j) and $(i,j{+}1)$, $\mathbf{n}_{i,j+1}$=$(s_y,-s_x)_{i,j+1}$ is the inward unit normal vector towards the i-line. The unit tangent vector towards the i-line is

$$\mathbf{s}_{i,j+1} = (\mathbf{r}_{i+1,j+1} - \mathbf{r}_{i-1,j+1})/|\mathbf{r}_{i+1,j+1} - \mathbf{r}_{i-1,j+1}|. \quad (6)$$

This grid block we call boundary cell layers. After calculating the metric tensor components g_{kl} at nodes of the i-lines j=$N_2{-}1$, $N_2{-}2,\ldots,N_2{-}j_o$, we specify components of the control metric tensor G_{kl}=g_{kl} at those nodes. If j_o=$N_2{-}2$ (it would imply that we specify all interior nodes), because the system (1) is universal, the numerical solution will reproduce the given mesh (see [10, 11]). This case may be represented as follows. The mesh, given on the domain $\mathcal{C}$ in the plane X,Y (see Fig. 2), is reproduced on the domain Ω in the plane x,y. If we specify only some upper part of the grid (j_o<$N_2{-}2$), due to the system (1) is elliptic, the initially given mesh in the plane X,Y will be distorted on the domain Ω.

Next, this block should be smoothly extended to the interior of the domain Ω. It may be done as follows. While moving in a j-line away from the boundary $\partial\Omega$, the tensor G_{kl} should be transformed to the identity tensor within j_1 nodes because in the interior of the domain Ω no additional control is needed. To this end, it is used a local mapping of 4 cells adjacent to the underlying node (see Fig. 1). The identity tensor at a node in the plane X,Y is specified by the 9-point square stencil of spacing 1. Consider the node (i,j), which is placed at the origin (0,0), and 8 adjacent nodes forming the 9-point stencil (see Fig. 3). For the initial stencil of Fig. 3, we define index j=$N_2{-}j_o$. Moving in the j-line from the node $(i,N_2{-}j_o{-}1)$ to the node $(i,N_2{-}j_o{-}j_1)$, we should gradually transform this stencil to the square stencil of spacing 1. To this end, the node $(i{-}1,j)$ should pass to the point $(-1,0)$, node $(i,j{-}1)$ to the point $(0,-1)$, etc., within j_1 cell layers. Let us introduce the local indices m,n=$-1,0,1$ for the 9-point stencil relating to the underlying node (i,j) so that m=$0,n$=0 specify the node (i,j); m=$1,n$=0 specify the node $(i{+}1,j)$; etc. Stencil transformation is performed using a linear interpolation

$$\mathbf{r}_{m,n} = \mathbf{r}^{\mathrm{in}}_{m,n} + \frac{N_2 - j_o - j}{j_1}\left(\mathbf{r}^{\mathrm{sq}}_{m,n} - \mathbf{r}^{\mathrm{in}}_{m,n}\right), \quad (7)$$

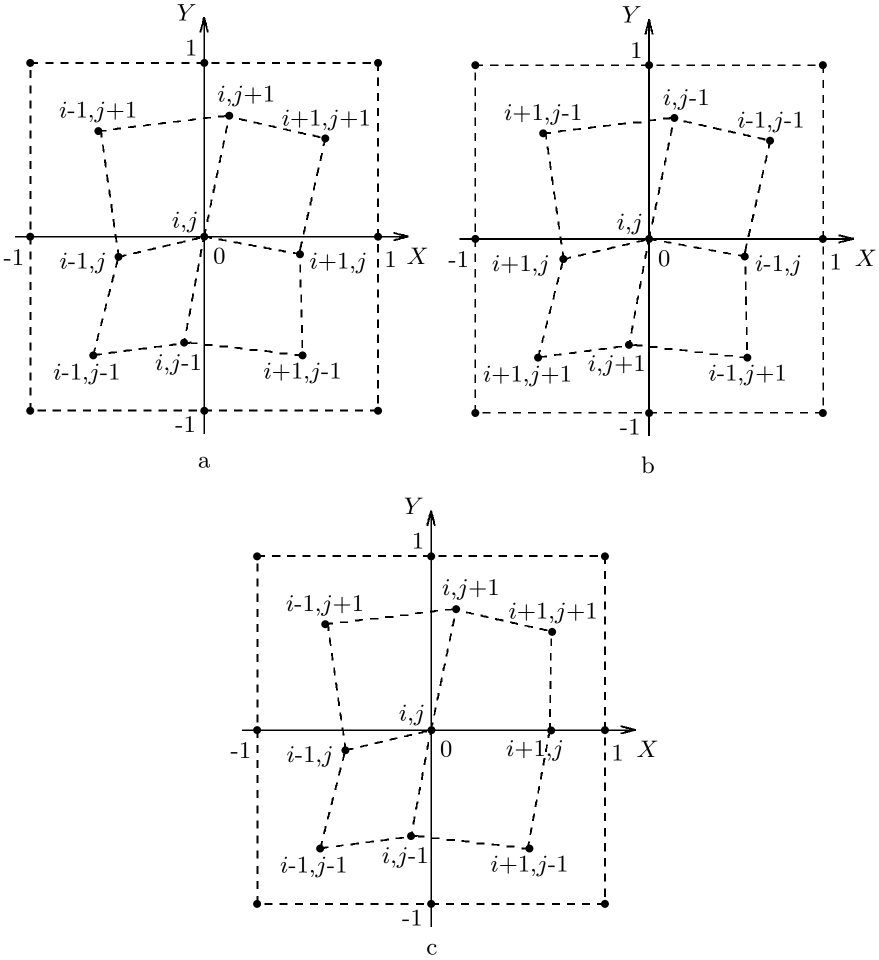

Fig. 3. Initial stencil transforms to square stencil of spacing 1. Correct location of initial stencil relatively square stencil (a), incorrect (b). Rotated stencil (c).

$$j{=}N_2{-}j_o{-}1, \ldots, N_2{-}j_o{-}j_1, \;\; m,n{=}{-}1,0,1,$$

where $\mathbf{r}^{\rm in}_{m,n}$ are the nodal coordinates of the initial stencil and $\mathbf{r}^{\rm sq}_{m,n}$ are the nodal coordinates of the square stencil of spacing 1, the node $m{=}n{=}0$ is fixed. Because the system (1) is invariant to rotation and scaling of the coordinates X, Y, the mesh constructed will smoothly transform to the grid on the rest of the domain Ω. However, the case depicted in Fig. 3b provokes 9-point stencil folding during transformation (7). To prevent this situation, first we rotate the initial stencil about the origin (0,0), i.e., about the point (i, j), so that the node $(i{+}1, j)$ lays in the X-axis (see Fig. 3c). We find the rotation angle φ between the vector $\mathbf{r}_{i+1,j}$ and X-axis

$$\cos\varphi = X_{i+1,j} \Big/ \sqrt{X_{i+1,j}^2 + Y_{i+1,j}^2}, \quad \sin\varphi = Y_{i+1,j} \Big/ \sqrt{X_{i+1,j}^2 + Y_{i+1,j}^2}$$

and update coordinates of 8 nodes

$$X'_{m,n}{=}X_{m,n}\cos\varphi{+}Y_{m,n}\sin\varphi,\ Y'_{m,n}{=}{-}X_{m,n}\sin\varphi{+}Y_{m,n}\cos\varphi,\ m,n{=}{-}1,0,1.$$

We obtain the stencil like that of Fig. 3c. Next, the transformation (7) is executed.

5 Mesh around airfoil

Consider the grid generation problem on the domain Ω around the NACA6409 airfoil represented parametrically with Bézier curves [18]

$$x(t) = F_1(Z_1(1-t)),$$
$$y(t) = \begin{cases} F_2(Z_1(1-t)) + Z_2(1-t,t_h), & \text{upper airfoil branch } y \ge 0 \ , \\ F_2(Z_1(1-t)) - Z_2(1-t,t_h), & \text{lower airfoil branch } y < 0 \ , \end{cases}$$
$$Z_1(t) = \sum_{i=1}^{8}\alpha_i B_i(t), \qquad Z_2(t,t_h) = t_h\sum_{i=1}^{8}\beta_i B_i(t),$$
$$F_1(t) = \sum_{i=1}^{4}\gamma_i C_i(t), \qquad F_2(t) = \delta\sum_{i=1}^{3} C_i(t),$$
$$0 \le t \le 1,\ \ t_h = 0.09,\ \delta = 0.12,\ \alpha_1 = 0,\ \alpha_2 = 0.03571,\ \alpha_3 = 0.10714,$$
$$\alpha_4 = 0.21429, \alpha_5 = 0.35714,\ \alpha_6 = 0.53571,\ \alpha_7 = 0.75,\ \alpha_8 = 1,\ \beta_1 = 0.18556,$$
$$\beta_2 = 0.34863,\ \beta_3 = 0.48919,\ \beta_4 = 0.58214,\ \beta_5 = 0.55724,\ \beta_6 = 0.44992,$$
$$\beta_7 = 0.30281,\ \beta_8 = 0.0105,\ \gamma_1 = 0.2,\ \gamma_2 = 0.4,\ \gamma_3 = 0.7,\ \gamma_4 = 1,$$
$$B_1(t) = 8t(1-t)^7,\ \ B_2(t) = 28t^2(1-t)^6,\ \ B_3(t) = 56t^3(1-t)^5,$$
$$B_4(t) = 70t^4(1-t)^4,\ \ B_5(t) = 56t^5(1-t)^3,\ B_6(t) = 28t^6(1-t)^2,$$
$$B_7(t) = 8t^7(1-t),\ B_8(t) = t^8,$$
$$C_1(t) = 4t(1-t)^3,\ C_2(t) = 6t^2(1-t)^2,\ C_3(t) = 4t^3(1-t),\ C_4(t) = t^4.$$

The outer domain boundary is specified by sides of the square $-1.5{\le}x{\le}2.5$, $-2{\le}y{\le}2$.

In Fig. 4, it is presented the O-type 105×51 mesh. The lines $i{=}1,N_1$ are coincide and go from the trailing edge, line $j{=}1$ is the outer domain boundary, line $j{=}N_2$ is the airfoil contour. In the upper airfoil branch, points are located by using the following distribution for the parameter t within the segment $0{\le}t{\le}1$

$$t_1 = 0,\ \ t_{i+1} = t_i + \triangle t_{i+1/2},\ i{=}1,2,\dots,N_a,\ N_a{=}(N_1{-}1)/2,$$
$$\triangle t_{3/2} = \frac{2\sigma}{(\sigma+1)N_a},\ \triangle t_{i+1/2} = \triangle t_{i-1/2} - \frac{2(\sigma-1)}{(\sigma+1)N_a(N_a-1)},\ i{=}2,3,\dots,N_a,$$

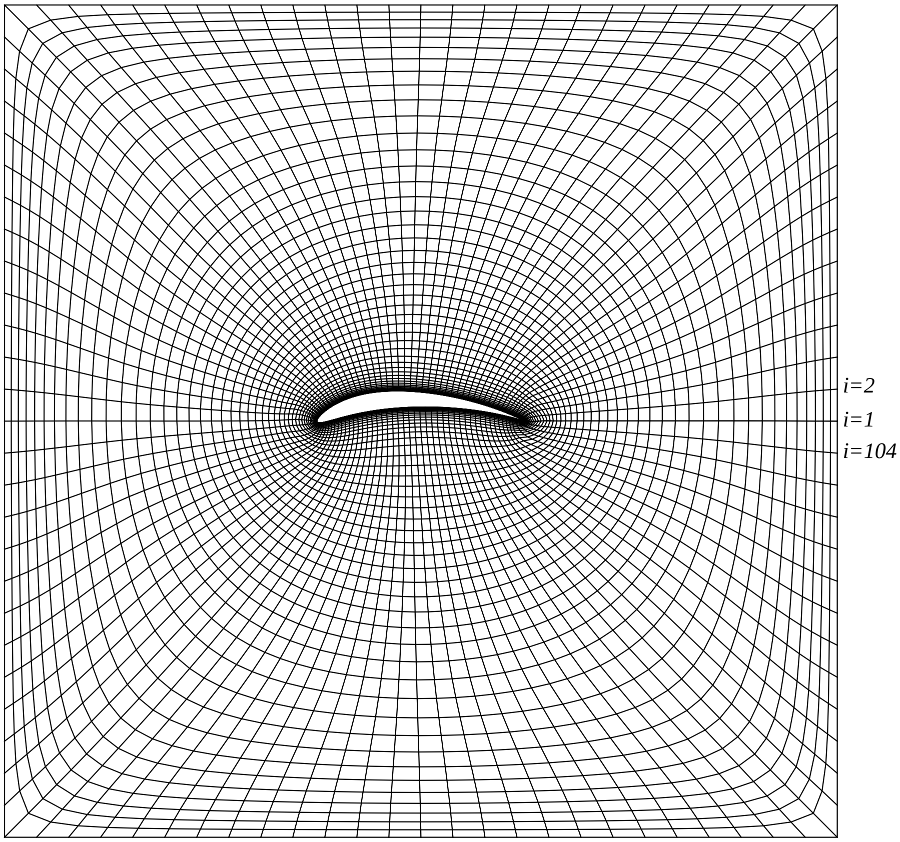

Fig. 4. 105×51 mesh with j-lines orthogonal to airfoil contour, mesh point clustering near airfoil and outer boundary.

where $\sigma{=}\triangle t_{N_a+1/2}/\triangle t_{3/2}{=}1/11.5$. For the lower airfoil branch points $i{=}N_a{+}2,\ldots,N_1{-}1$, the above formulae are utilized with $\sigma{=}\triangle t_{N_a+3/2}/\triangle t_{N_1-1/2}{=}0.1$.

In a neighborhood of the trailing edge, the continuous mapping is unstable that causes grid lines to overlap. To prevent grid folding we imply a constrain. It is that the line $i{=}1$ should approach the corner point along the bisectrix of the trailing edge outer angle. Several nodes of the line $i{=}1$ lay in the bisectrix, i.e., at iterations (4) the shift vector $\mathbf{r}^{l+1}_{1,j} - \mathbf{r}^{l}_{1,j}$ is projected to the bisectrix.

To satisfy the conditions of orthogonality and clustering near the airfoil contour we define the control metric G in the following manner. In the plane X, Y we specify nodal coordinates $\mathbf{r}_{i,j}{=}(X,Y)_{i,j}$ of j_o cell layers according to the formula (5) with mesh spacings along the j-line

$$h_{i,j+1/2} = h_{i,N_2-1/2} + \big[(N_2-1-j)/j_o\big]^2 (h_{i,N_2-j_o+1/2} - h_{i,N_2-1/2})\,,$$
$$i{=}1,2,\ldots,N_1,\ j{=}N_2{-}1,...,N_2{-}j_o,$$

where $h_{i,N_2-1/2}, h_{i,N_2-j_o+1/2}$ are given spacings in the 1st and j_oth (from airfoil contour) boundary cell layers. In Fig. 5, the boundary cell layers are presented in the plane X, Y with parameters j_o=20, $h_{i,N_2-1/2}$=0.03, $h_{i,N_2-j_o+1/2}$=6·10^{-3}. These layers may be considered as a part of the mesh on the domain $\mathcal{C}$. The line i=1 is the bisectrix of the trailing edge outer angle

$$\mathbf{r}_{1,j} = \mathbf{r}_{1,j+1} + \mathbf{b}\, h_{1,j+1/2}\,, \quad j{=}N_2{-}1, ..., N_2{-}j_o\,. \tag{8}$$

Here with $j{=}N_2{-}1, \ldots, N_2{-}j_b$ the unit vector $\mathbf{b}{=}\mathbf{b}_d$ specifies the bisectrix and number of gird nodes j_b in this bisectrix is changed depending on node clustering toward airfoil, see Table 1.

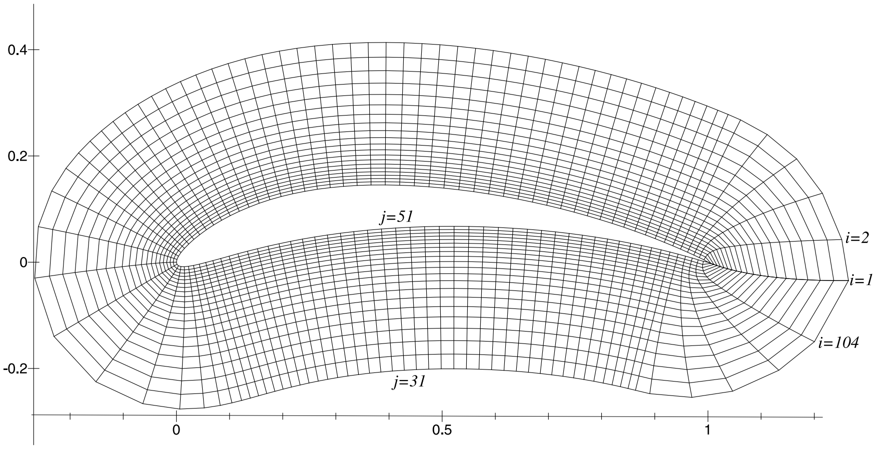

Fig. 5. Boundary cell layers in plane X, Y.

Table 1. Parameters of mesh on $\mathcal{C}$ domain in X, Y plane

$h_{i,N_2-1/2}$	$6{\times}10^{-3}$	$3{\times}10^{-3}$	10^{-3}	$3{\times}10^{-4}$	10^{-4}	$3{\times}10^{-5}$	10^{-5}
$h_{i,N_2-j_o+1/2}$	0.03	0.02	0.02	0.02	0.02	0.02	0.02
j_b	1	3	4	6	8	8	8

For the rest of nodes in the line i=1 the vector $\mathbf{b}$ in (8) specifies the direction which changes smoothly from $\mathbf{b}_d$ to the vector $\mathbf{k}$=(1, 0)

$$\mathbf{b} = \frac{\tilde{\mathbf{b}}}{|\tilde{\mathbf{b}}|}\,, \quad \tilde{\mathbf{b}} = \mathbf{b}_d + \frac{N_2 - j_b - j - 1}{j_o - j_b - 1}(\mathbf{k} - \mathbf{b}_d), \; j{=}N_2{-}j_b{-}1, \ldots, N_2{-}j_o\,.$$

Near the airfoil, direction of the lines i=1, 2 as well as i=105, 104 changes sharply, nearly by 90^o. This causes quality of the mesh on Ω deteriorates. We smooth this change of direction by using a vector $\mathbf{t}_{i,j+1}$, a normalized linear combination of $\mathbf{n}_{i,j+1}$ and $\mathbf{b}$, instead of the normal vector $\mathbf{n}_{i,j+1}$ in the formula (5)

$$\mathbf{t}_{i,j+1}=\frac{\tilde{\mathbf{t}}_{i,j+1}}{|\tilde{\mathbf{t}}_{i,j+1}|}\,,\quad \tilde{\mathbf{t}}_{i,j+1}{=}\lambda_i\mathbf{n}_{i,j+1}+\mathbf{b},\ \ i{=}2,\ldots,4,N_1{-}4,\ldots,N_1{-}1,\ \ \lambda_2{=}1.5,$$
$$\lambda_3{=}2.7,\ \ \lambda_4{=}4.5,\ \ \lambda_5{=}10,\ \ \lambda_{N_1-4}{=}5,\ \ \lambda_{N_1-3}{=}3,\ \ \lambda_{N_1-2}{=}1.2,\ \ \lambda_{N_1-1}{=}0.5,$$

with indices $j{=}N_2{-}j_b{-}1,\ldots,N_2{-}j_o$. With indices $j{=}N_2{-}1,N_2{-}2$, we use the normal vectors $\mathbf{n}_{i,j+1}$ in the formula (5) with all $i{=}2,\ldots,N_1{-}1$. For the lines $j{=}N_2{-}3,...,N_2{-}j_b$ we use a vector $\mathbf{p}_{i,j+1}$, a normalized linear combination of $\mathbf{n}_{i,j+1}$ and $\mathbf{t}_{i,j+1}$, instead of the vector $\mathbf{n}_{i,j+1}$ in the formula (5)

$$\mathbf{p}_{i,j+1}=\frac{\tilde{\mathbf{p}}_{i,j+1}}{|\tilde{\mathbf{p}}_{i,j+1}|}\,,\quad \tilde{\mathbf{p}}_{i,j+1}=\mathbf{n}_{i,j+1}+\frac{N_2-2-J}{5}(\mathbf{t}_{i,j+1}-\mathbf{n}_{i,j+1}),$$
$$i=2,...,5,N_1{-}4,...,N_1{-}1.$$

The mesh of Fig. 5 is the boundary cell layers of an initial grid in the iterative procedure (4). The remained part of the initial grid may be produced, for instance, by an algebraic method. Transformation (7) of the tensor G_{kl} to the identity tensor is executed within $j_1{=}6$ cell layers. We calculate the metric tensor G_{kl} for every new parameters $h_{i,N_2-1/2}$, $h_{i,N_2-j_o+1/2}$ of Table 1. After implementing iterations (4), the resulting mesh is used as an initial guess for the grid with new parameters $h_{i,N_2-1/2}$, $h_{i,N_2-j_o+1/2}$ except for j_o boundary cell layers for which the initial mesh is the grid on the domain $\mathcal{C}$. For the first 1000 iterations (4) we set the iterative parameter τ equal to 0.3 and for the remained iterations $\tau{=}1.7$. The parameter ε, serving for stopping iterations, is equal to 10^{-14}. Convergence is attained within 2500 to 3000 iterations.

Fig. 6 presents fragments of the grid on Ω (for entire mesh see Fig. 4) with the fifth set of parameters of the Table 1. For the last set of parameters of the Table 1 in all cells of the layer $j{=}N_2{-}1$ (nearest to airfoil), the spacing $h_{i,N_2-1/2}$ is exactly equal to 10^{-5}. The angle φ between j-line and tangent vector towards the airfoil contour at the node (i,N_2), $i{=}2,...,N_1{-}1$, computed via (6), is equal to 90^o with a deviation $|\triangle\varphi|{\le}0.1^o$. Thus, the requirements of mesh orthogonality and prescribed node clustering near the airfoil are obeyed.

Besides we regulate the cell shape near the outer boundary. The control metric tensor G_{kl} is specified by the rectangular grid on the domain $\mathcal{C}$ with spacing in the X- and Y-axis

$$X_{i+1,j}-X_{i,j}=h^x_{i+1/2}=1,\quad i{=}1,\ldots,N_1{-}1,\ j{=}1,\ldots,j_2,$$
$$Y_{i,j+1}{-}Y_{i,j}{=}h^y_{j+1/2}{=}h^y_{j_2-1/2}{+}\left[\frac{j{-}1}{j_2{-}1}\right]^q(1{-}h^y_{j_2-1/2}),\ i{=}1,\ldots,N_1,\ j{=}1,\ldots,j_2.$$

The parameters are $j_2{=}11$, $q{=}1.5$, $h^y_{j_2-1/2}{=}0.3$ for the mesh of Fig. 4. In general, the spacing $h^y_{j+1/2}$ may also depend on the index i.

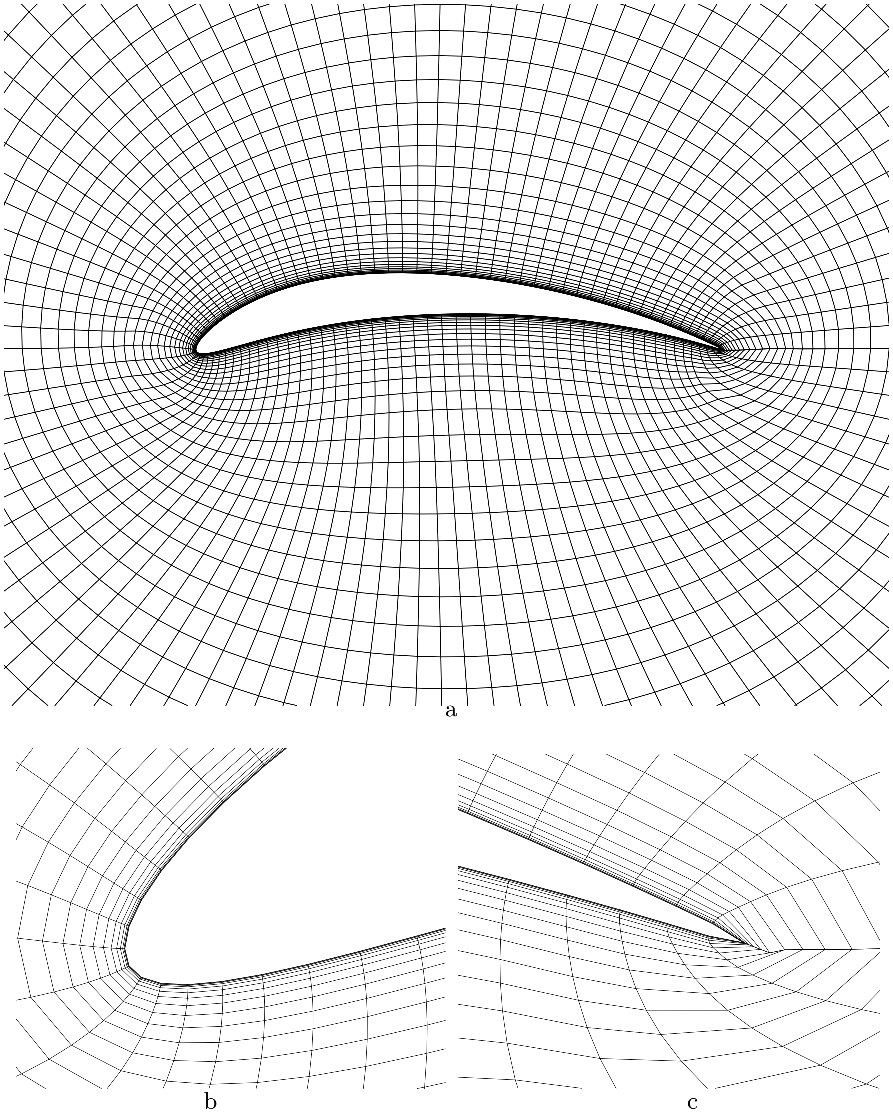

Fig. 6. Close-up with magnification factor of 3 (a) and 50 (b),(c).

6 Conclusion

We presented the grid construction method by using the quasi-conformal mapping. Existence and uniqueness of a diffeomorphic harmonic mapping is provided by the Radó theorem for the inverted Laplace equations. Next, this mapping is deformed so that to obtain a grid with required properties. The universal elliptic PDEs allow to obey the conditions of orthogonality and prescribed mesh point clustering near the domain boundary. The technique of specifying the control metric was considered. For this, two formulations of grid generation problem were used with implementing a local additional mapping and a global additional mapping.

Acknowledgement

This work was supported by the Department of Mathematical Sciences of the Russian Academy of Sciences (Program 3) and Russian Foundation for Basic Research (project code 09-01-00173).

References

1. Steger, J.L., Chausse, D.S.: Generation of body-fitted coordinates using hyperbolic partial differential equations. SIAM Journal on Scientific Computing 1(4), 431–437 (1979).
2. Visbal, M., Knight, D.: Generation of orthogonal and nearly orthogonal coordinates with grid control near boundaries. AIAA Journal, 20(3), 305–306 (1982).
3. Prokopov, G.P.: Some general issues of grid generation algorithms. VANT. Ser. Mathematical modelling of physical processes. 1, 37–46 (1998) (in Russian).
4. Winslow, A.M.: Numerical solution of the quasi-linear Poisson equation in a nonuniform triangle mesh. J. Comput. Phys. 1, 149–172 (1966).
5. Godunov, S.K., Prokopov, G.P.: The use of moving meshes in gasdynamics computations. USSR Comput. Maths. Math. Phys. 12(2), 182–191 (1972).
6. Thompson, J.F., Mastin, C.W., Thames, F.C.: Automatic numerical generation of body-fitted curvilinear coordinate system for field containing any number of arbitrary two-dimensional bodies. J. Comp. Phys. 15, 299–319 (1974).
7. Radó, T.: Aufgabe 41, Jahresber, Deutsche Math.-Verein 35, 49 (1926).
8. Roache, P.J., Steinberg, S.: A new approach to grid generation using a variational formulation, AIAA Paper, No. 85-1527-CP, AIAA 7th Computational Fluid Dynamics Conference, Cincinnati, OH, July, 1985.
9. Knupp, P., Luczak, R.: Truncation error in grid generation: a case study. Numer. Meth. Part. Dif. Eq. 11, 561–571 (1995) .
10. Azarenok, B.N.: Generation of structured difference grids in two-dimensional nonconvex domains using mappings. Comput. Math. Math. Phys. 49(5), 797–809 (2009).
11. Azarenok, B.N.: On 2D structured mesh generation by using mappings. Numerical Methods for Partial Differential Equations. (2010) Published online in Wiley InterScience (www.interscience.wiley.com). DOI 10.1002/num.20570.
12. Thompson, J.F., Thames, F.C., Mastin, C.W.: TOMCAT - a code for numerical generation of boundary-fitted curvilinear coordinate systems on fields containing any number of arbitrary two-dimensional bodies. J. Comp. Phys. 24, 274–320 (1977).
13. Spekreijse, S.P.: Elliptic grid generation based on Laplace equations and algebraic transformations. J. Comput. Phys. 118, 38–61 (1995).

14. Ivanenko, S.A.: Control of cell shape in the construction of a grid. Comput. Math. Math. Phys. 40(11), 1596–1616 (2000).
15. Sidorov, A.F., Shabashova, T.I.: On one method of computation of optimal difference grids for multidimensional domains. Chisl. Metody Mechaniky Sploshnoy Sredy. 12, 106–123 (1981) (in Russian).
16. Steger, J.L., Sorenson, R.L.: Automatic mesh-point clustering near a boundary in grid generation with elliptic partial differential equations. J. Comp. Physics 33, 405–410 (1979).
17. Kaul, U.K.: New boundary conditions for elliptic systems used in grid generation problems. J. Comp. Physics. 189, 476–492 (2003).
18. Boehm, W.: Bézier presentation of airfoils. Computer Aided Geometric Design. 4, 17–22 (1987).